High-Throughput Graphene Imaging on Arbitrary Substrates with Widefield Raman Spectroscopy

Robin W. Havener,[†,¶] Sang-Yong Ju,[‡,§,¶] Lola Brown,[‡] Zenghui Wang,[‡] Michal Wojcik,[‡] Carlos S. Ruiz-Vargas,[†] and Jiwoong Park[‡,⊥,*]

[†]Department of Applied and Engineering Physics, [‡]Department of Chemistry and Chemical Biology, and [⊥]Kavli Institute at Cornell for Nanoscale Science, Cornell University, Ithaca, New York 14853 and [§]Department of Chemistry, Yonsei University, Seoul 120-749, Republic of Korea [¶]These authors contributed equally to this work.

ABSTRACT

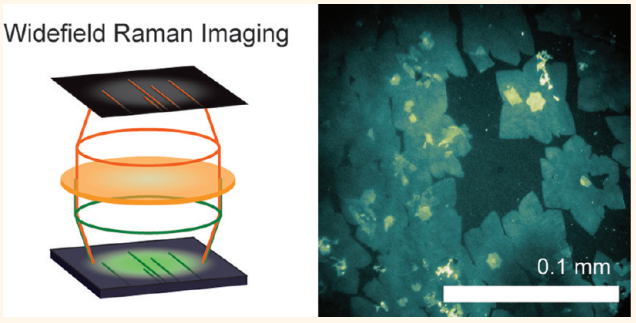

Raman spectroscopy has been used extensively to study graphene and other sp^2-bonded carbon materials, but the imaging capability of conventional micro-Raman spectroscopy is limited by the technique's low throughput. In this work, we apply an existing alternative imaging mode, widefield Raman imaging (WRI), to image and characterize graphene films on arbitrary substrates with high throughput. We show that WRI can be used to image graphene orders of magnitude faster than micro-Raman imaging allows, while still obtaining detailed spectral information about the sample. The advantages of WRI allow characterization of graphene under conditions that would be impossible or prohibitively time-consuming with other techniques, such as micro-Raman imaging or reflected optical microscopy. To demonstrate these advantages, we show that WRI enables graphene imaging on a large variety of substrates (copper, unoxidized silicon, suspended), large-scale studies of defect distribution in CVD graphene samples, and real-time imaging of dynamic processes.

KEYWORDS: graphene · Raman · imaging · spectroscopy · widefield

Graphene, a single sheet of sp^2-bonded carbon atoms, has attracted enormous attention due to its unique electrical and optical properties and high mechanical strength.[1] Large-scale graphene production has recently been achieved through chemical vapor deposition (CVD) on metallic substrates,[2,3] but CVD grown graphene samples can vary greatly in terms of number of layers, grain size, and defect density. To optimize growth conditions and fabricate large-scale devices on-chip, it is necessary to map and characterize large areas of graphene during device fabrication. White-light reflection optical microscopy is a simple and rapid technique for identifying graphene on a sample, but it can only be used on certain substrates (such as silicon with a specific oxide thickness[4]). Other imaging modalities, such as fluorescence-based imaging[5] and fluorescence quenching microscopy,[6] have recently been developed to overcome this limitation, but provide almost no information about graphene quality. To this end, Raman spectroscopy has been used extensively to probe sp^2-bonded carbon materials, providing information about defect or dopant density,[7−12] mechanical strain,[13] electron−phonon interactions,[7,11,14] and number of graphene layers.[3,9,12,15] To study materials on a substrate, Raman measurements are typically performed in a confocal geometry, where detailed spectral information can be obtained at the location of a focused laser spot (Figure 1A).

However, spatial mapping of a sample with confocal micro-Raman is limited due to the technique's low throughput. To create an image, the laser spot is raster-scanned across the sample to generate a two-dimensional map of a specific Raman band (see Figure 1A for a schematic). The image acquisition speed is limited by the low efficiency of Raman scattering and the laser power (restricted by the damage threshold, below 2 mW for confocal illumination of graphene[16]). As a result, a diffraction-limited image of an area of tens of micrometers across typically requires hours to acquire, making micro-Raman ill-suited for rapid large-scale imaging of graphene.

Another alternative is to employ widefield Raman imaging (also known as global or direct Raman imaging),[17−22] which is illustrated in Figure 1B. In this imaging

* Address correspondence to jpark@cornell.edu.

Received for review September 28, 2011 and accepted December 21, 2011.

Published online December 29, 2011
10.1021/nn2037169

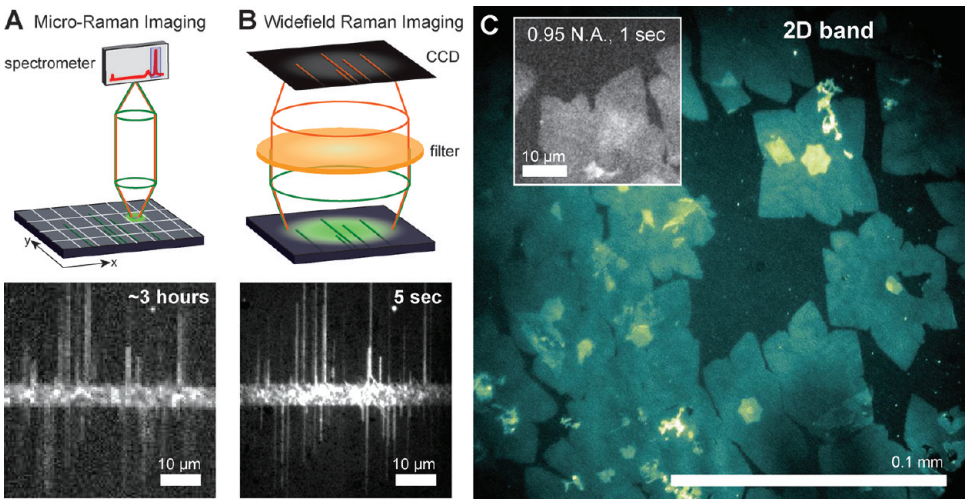

Figure 1. Comparison of two-dimensional scanning confocal Raman (A) with widefield Raman imaging (WRI, B). Schematics illustrate a serial collection of spectra over a series of pixels with a confocal micro-Raman setup (A) *vs* large area imaging of a specific band with the widefield Raman imaging setup (B). Below are G band images of the same area of aligned carbon nanotubes obtained with (A) micro-Raman setup (~3 h acquisition, 0.5 μm pixel size) and (B) widefield Raman setup (5 s acquisition, *ca.* 80 μm illumination size, 3 W), using 100× objective (N.A. = 0.95) in both cases. (C) A submillimeter scale false color 2D band image of graphene using 20× objective (N.A. = 0.70) with 300 s acquisition time. (inset) With a 100× (N.A. = 0.95) objective, graphene is clearly visible on Si/285 nm SiO_2 at acquisition times as short as 1 s. Image is Gaussian blurred (radius 1 pixel = 125 nm) to reduce CCD noise.

mode, a planar sample is illuminated with a large collimated (or defocused) laser spot, and the Raman-scattered light from the entire illuminated area is imaged with an objective lens and a CCD camera after filters select for a specific Raman band. The laser power used to illuminate the sample can be orders of magnitude stronger than that used in micro-Raman imaging, but the power is distributed over a much larger area, preventing damage to the sample. This allows for rapid acquisition of large-area, diffraction-limited images. Additionally, imaging spectroscopy can be used in a line mapping geometry to obtain high spectral resolution Raman spectra once an area of interest is identified (see Figure 2).[20,23] Widefield Raman imaging (WRI) has been successfully employed for a variety of applications in chemistry, biology, and materials science.[17−20]

Applying this existing technique to image graphene and other sp^2-bonded carbon materials on planar substrates is straightforward. Widefield Raman images can be acquired at wavelengths corresponding to the known Raman bands of these materials (G, D, 2D) by using the appropriate optical bandpass filters.[17−20] However, despite the fact that Raman spectroscopy is used to characterize sp^2-bonded carbon materials so frequently, WRI was only recently applied to carbon nanotube imaging,[21,22] and the time-consuming micro-Raman technique is still the standard tool for Raman imaging of graphene. In this paper, we first demonstrate that WRI indeed enables rapid, large-scale, and nondestructive characterization of graphene, while providing spectral information comparable to that obtainable with confocal Raman. Then we showcase the advantages of WRI in three important applications described below, which establish WRI as a powerful and versatile characterization method for graphene at different stages of growth and device fabrication.

First, we show that unlike white-light optical microscopy, widefield Raman imaging can be used to rapidly and clearly visualize graphene on a variety of substrates, including unoxidized silicon and copper, as well as suspended graphene. Second, we demonstrate that WRI is a valuable tool to characterize the quality of CVD graphene, revealing spatial inhomogeneities in film quality that could easily go undetected with point Raman spectroscopy. Finally, we use WRI to monitor dynamic processes in graphene with high spatial and spectral resolution over a large area in real time. These novel implementations of WRI for graphene imaging provide valuable information that cannot be easily obtained with other optical imaging methods, and enable new experiments at various stages of graphene growth and processing.

RESULTS AND DISCUSSION

We illustrate in Figures 1 and 2 that widefield Raman imaging enables high-throughput, diffraction-limited imaging, and spectroscopy of graphene and other sp^2-bonded carbon materials (see Methods and Supporting Information for details about our experimental setup). First, to demonstrate the difference in imaging capabilities between WRI and micro-Raman imaging, Figure 1 panels A and B show G band images of aligned single-walled carbon nanotubes on a quartz substrate (see Methods for sample preparation) obtained using micro-Raman imaging and WRI, respectively. The WRI image was obtained in 5 s (3 W total laser power with a 80 μm

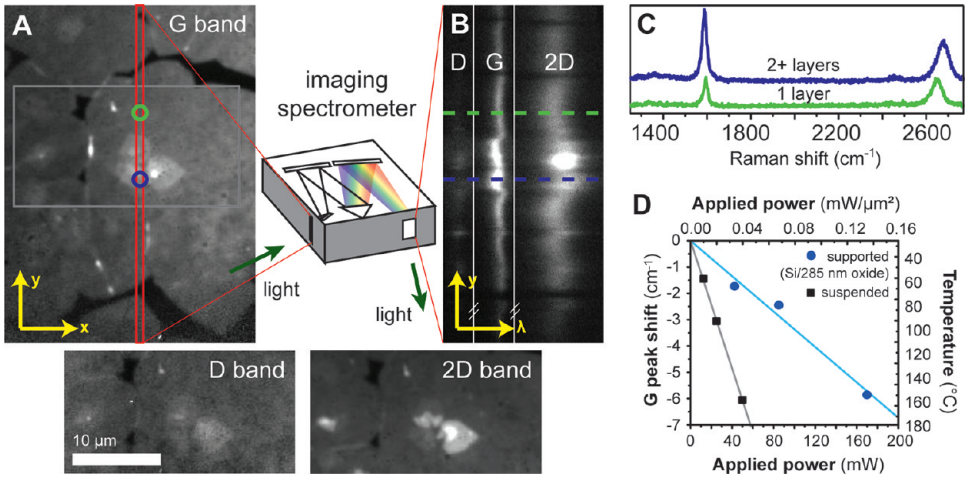

Figure 2. (A) (Top) G band image of CVD graphene that has been normalized for spatial variations in laser intensity (using the second order silicon Raman peak, see Supporting Information). Red box indicates a kinematic slit position for spectral measurement. (Bottom) Normalized D and 2D band images of area outlined in G band image, obtained with tunable bandpass filter. (B) Spectral analysis along the line in image A, with D, G, and 2D Raman bands visible. Note that the abscissa changes from distance to Raman shift. Spectra were obtained in 60 s with spectrometer entrance slit width of 50 μm (3.5 cm^{-1}) and 500 mW laser power over an ~80 μm spot size. (C) Raman spectra for single (bottom) and multiple (top) graphene layers, obtained along dotted lines in image B. (D) Approximate temperature increase of graphene *vs* applied power for a suspended (black) and supported (blue) graphene sample. G peak shift is determined by offsetting the linear fit of G peak position *vs* applied power to 0 at room temperature (25 °C).

spot size), while the confocal Raman image took 3 h (0.5 μm pixel size and 1 s/pixel). Despite its much shorter acquisition time (~1/2000), the WRI image has a better signal-to-noise ratio and improved spatial resolution. We also stress that the inherent resolution of WRI is diffraction-limited, whereas increasing the resolution of a micro-Raman image requires more pixels, and thus a longer imaging time.

Figure 1C shows a submillimeter scale false color image of the 2D band of CVD graphene with intentionally incomplete surface coverage (see Methods) transferred onto a Si/285 nm oxide substrate. This image was obtained with a 20× objective (numerical aperture, N.A. = 0.70), 50 mW of laser power at 532 nm, and an acquisition time of 300 s. A confocal image on this scale with identical imaging conditions as in Figure 1A would take 35 h to obtain. Using an objective with a higher N.A. (0.95, 100×), we can further decrease the imaging time, allowing the graphene film to be resolved in as little as 1 s (see inset). High-quality images can be obtained on Si/285 nm oxide in 1 min under these imaging conditions.

Spectral information about the sample can be obtained with various bandpass filters. Figure 2A shows G, D, and 2D band images of the same area of a large grain CVD-grown graphene sample transferred onto a Si/285 nm oxide substrate (500 mW power with a 80 μm spot size). We used a custom-made, continuously variable filter for this purpose, with a bandwidth of 100 cm^{-1} (~3 nm) for 940−1850 cm^{-1} (see Methods), encompassing the D and G bands. This technique allows for rapid comparison of the relative intensities of these Raman bands over large areas. From the data shown in Figure 2A, we can observe graphene nucleation sites and growth patterns with a high signal-to-noise ratio, and we find that our sample has a relatively low defect density over a large area.

For high-resolution spectral information, we can perform imaging spectroscopy.[20,23] While maintaining widefield illumination, Raman spectra along a vertical line on the sample can be obtained by positioning the entrance slit of a spectrometer at the image plane. Figure 2 panels B and C present Raman spectra acquired in this mode. Here, the *y*-axis of the CCD image after the imaging spectrometer (Figure 2B) corresponds to the *y*-axis of the real space image along a fixed line (Figure 2A), while the *x*-axis of the CCD image corresponds to the Raman shift (cm^{-1}). Multilayer areas can be rapidly identified from an abrupt increase in G band intensity[24] and redshift of the 2D peak,[12] which can be confirmed quantitatively by extracting Raman spectra from the CCD data (Figure 2C). In addition, we observe small (*ca.* ±2 cm^{-1}) fluctuations in the G peak position, which could indicate local doping[10] or strain[13] in our sample. All of the data in Figure 2 were acquired in a matter of minutes, providing a means to rapidly characterize the quality of CVD graphene over a large area. In addition, collecting a series of such spectra while scanning the sample in the *x*-direction ("line mapping") allows for complete sample mapping with full Raman spectra at every point.[20,23] Since data from many pixels are still acquired in parallel, this technique provides the same information that can be acquired with confocal micro-Raman imaging in a much shorter time.[20]

Finally, to ensure that graphene is not damaged by WRI, we monitor the local temperature increase induced by the imaging laser. Heating graphene in an

oxidative environment (such as air) can cause strong hole doping at ~200 °C and etching at 450 °C,[25] so to avoid damage, the sample should be kept below these temperatures. We can estimate the temperature increase of the graphene by measuring the G peak position as a function of laser power, and using a known conversion factor between G peak position and temperature.[26] Our results for supported graphene (on silicon/285 nm oxide), as well as suspended graphene (see Figure 3), are shown in Figure 2D. For suspended samples, or supported samples at higher powers, the temperature increase can be significant. However, under the conditions used to image most of our samples (50 mW over a 40−50 μm spot size), the local temperature only increases by a few tens of degrees Celsius, confirming that WRI provides both rapid and nondestructive graphene imaging. From Figures 1 and 2, it is clear that WRI is well-suited for high-throughput graphene imaging and characterization.

Next, we demonstrate several unique applications of WRI for graphene monitoring and research which would be difficult or impossible with other imaging techniques. First, we show that WRI can be used to rapidly visualize graphene on a large variety of substrates, enabling high-throughput characterization through various stages of graphene growth and device fabrication. Previous work employing WRI to image carbon nanotubes focused mainly on suspended nanotubes,[21,22] which typically exhibit stronger Raman scattering than nanotubes on a substrate,[21,27] and imaging of graphene is often performed on silicon with a 285 nm thick oxide layer, which enhances optical contrast through constructive interference.[4,24] However, graphene exhibits a similar Raman signature on many substrates,[28] allowing substrate-independent Raman imaging. Although the intensity of the Raman signal is reduced on the substrates we studied as compared to silicon/285 nm oxide, good quality raw images on all of these substrates can be acquired in 5 min or less.

First, as with carbon nanotubes,[21,22] WRI can be used to image suspended regions of graphene. Figure 3A shows an optical image (left) of a bare silicon substrate with 5 μm square holes etched through it. CVD graphene was transferred on top of the substrate, but it is impossible to resolve under a white light reflection microscope. On the other hand, a 2D band WRI image (right) quickly reveals that most of the holes are covered in graphene. Suspended graphene can be visualized with an acquisition time of seconds (see Figure 5), while high quality images like Figure 3A can be obtained in 1−2 min.

The Raman signal is approximately an order of magnitude stronger over the suspended regions than it is on bare silicon (see Figure 3A, inset). Even on bare silicon, however, graphene can be resolved with WRI using a sufficiently long collection time (300 s). WRI can easily resolve the edges and multilayer regions of graphene on silicon, as shown in Figure 3B, even though the graphene is very difficult to distinguish in an optical image. WRI can also image

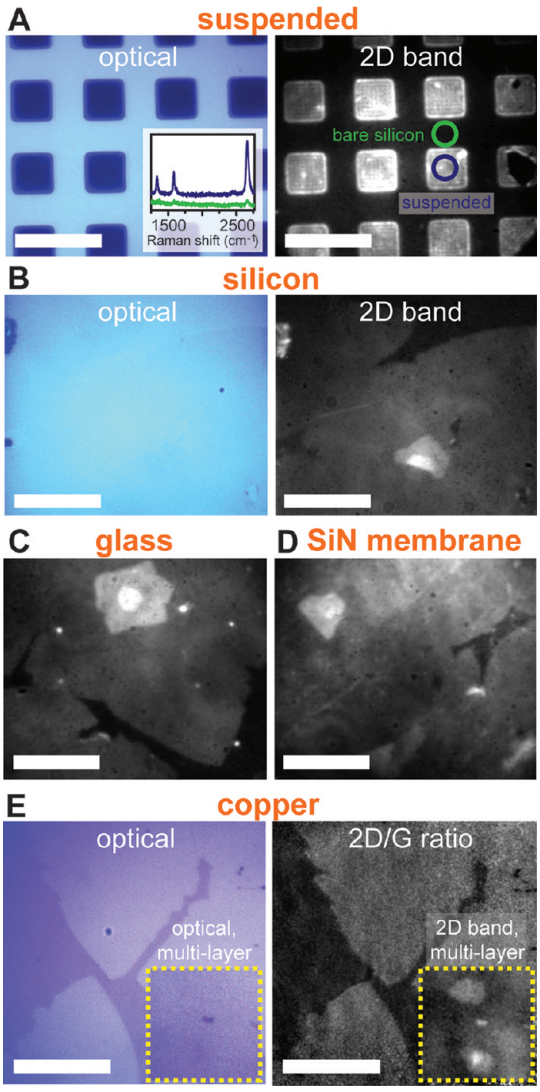

Figure 3. (A) (Left) Optical image of graphene suspended over 5 μm holes etched in bare silicon. The graphene is invisible over the entire substrate. (Right) 2D band image of the same area shows a high yield of suspended graphene. Acquisition time 60 s at 50 mW power over a ~50 μm spot size. (Inset) Raman spectra from suspended and supported graphene. The intensity of the Raman signal of supported graphene on bare silicon is an order of magnitude smaller than the signal of suspended graphene. (B) (Left) Optical image of graphene on bare silicon, which is also almost impossible to see. (Right) 2D band image of same area shows graphene edges and multilayer areas. Acquisition time 300 s at 50 mW power. (C) 2D band image of graphene on fused silica, acquisition time 300 s at 50 mW power. (D) 2D band image of graphene on 5 nm thick silicon nitride, acquisition time 300 s at 50 mW power. (E) (Left) Optical image of graphene grown on copper film. Inset shows an area with multiple graphene layers, which is indistinguishable from single-layer graphene. (Right) 2D/G ratio image (see Supporting Information) shows location of graphene on copper, and multiple layer regions (inset, same area as optical image) can be distinguished from single-layer ones in a 2D band image. Raw images acquired in 300 s with 450 nm laser at 50 mW power. All scale bars are 10 μm.

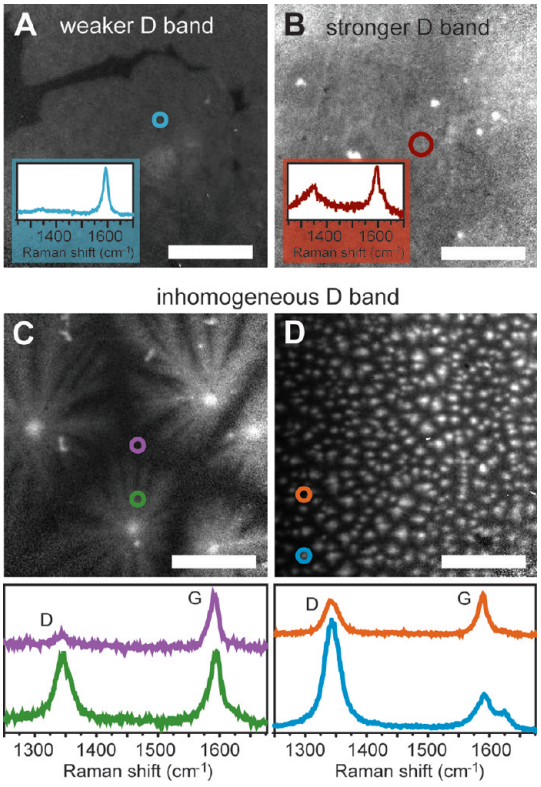

Figure 4. Normalized D band images of various graphene samples (see Methods for growth parameters) transferred to Si/285 nm oxide. Samples exhibit a large variety of behaviors with respect to D band intensity. Some samples (A) exhibit very low, uniform D band intensity, while others (B) exhibit higher, uniform intensity. Insets show point Raman spectra, which are representative of the sample as a whole. Other samples, however, have large spatial variations in D band intensity. Images C and D are two examples of such behavior. Point Raman spectra taken at different locations on the sample (shown below C, D) can appear very different. All scale bars are 10 μm.

graphene on transparent substrates, such as glass (Figure 3C), and on 5 nm thin silicon nitride membranes (Figure 3D), allowing subsequent dark field TEM studies.[29]

Lastly, WRI can be used to visualize CVD graphene directly on its copper growth substrate, which allows confirmation of graphene growth without transfer. Under white light illumination (Figure 3E, left), graphene shows a slight contrast difference from the copper substrate. Likely, the bare copper is slightly oxidized, while the graphene-covered areas are protected from oxidation.[30] Multilayer regions of graphene (inset) are indistinguishable from single-layer ones. Copper exhibits photoluminescence[31] which contributes a background to the Raman signal, but we find that with a 450 nm excitation wavelength, graphene can still be visualized on copper using WRI. A 2D/G ratio image (see Supporting Information) clearly distinguishes graphene from bare copper (Figure 3E, right), and multilayer regions can be identified in a 2D band image (inset). Thus, WRI can be used to locate and characterize graphene after all stages of device fabrication—growth, transfer to a target substrate, and patterning—and provides extra flexibility.

As a second application of WRI, we demonstrate that D band imaging can be used to rapidly compare the quality of large areas of CVD graphene produced with different growth conditions. The intensity of the Raman D peak (~1350 cm^{-1}) scales with the density of defects in a graphene film,[8] and a low D peak (or low D/G intensity ratio) usually indicates a high quality film. Often, point Raman spectroscopy or confocal mapping over a relatively small area is used to characterize the D peak of CVD graphene, but with WRI, we can rapidly image the D band intensity directly on a large scale. After transferring graphene to Si/285 nm oxide, we find that for some samples (Figure 4A,B), the D band intensity is roughly constant over tens of micrometers, and can be well-described with point Raman spectra (see insets). However, other samples (Figure 4C,D) show large spatial inhomogeneities in D band intensity (see Methods for growth parameters). Raman spectra taken at various points on the sample can have vastly different D/G intensity ratios, as shown in Figure 4.

It is unknown whether these inhomogeneities in D band are due to varying grain sizes, atomic defects, or larger-scale debris. Transferring these samples to silicon nitride membranes (as in Figure 3D) will allow us to combine widefield Raman spectroscopy with dark field TEM imaging for future experiments that correlate grain size and D band intensity over a large scale. Currently, however, it is clear that point Raman spectroscopy is not sufficient to fully characterize the quality of a CVD graphene film, and that WRI provides valuable information about the spatial distribution of defects in our samples.

Finally, WRI can capture images within fractions of a second, allowing large-scale, real-time spatially and spectrally resolved imaging of dynamic processes specific to graphene. We demonstrate the dynamic capability of WRI by using the imaging laser at a high power to damage the graphene, and observing the process in real time. When graphene is suspended (see Figure 3), 50 mW of laser power can cause the graphene to tear. By taking 2D band images rapidly (0.5 s frame rate), we can observe the dynamics of this process. Figure 5A shows a 2D band image of a suspended graphene film. After the laser power is increased, a hole is formed in the film and grows quickly, causing the entire film to fail within a few seconds (see Supporting Information for full movie).

From Figure 2D, we note that the temperature of the graphene remains below the damage threshold of 200 °C, even at 50 mW laser power. However, the mechanical failures we observe appear to propagate from point defects and edges, which could be particularly unstable at higher temperatures. In addition, optical forces have been shown previously to manipulate carbon nanotubes,[21] and may also be manipulating

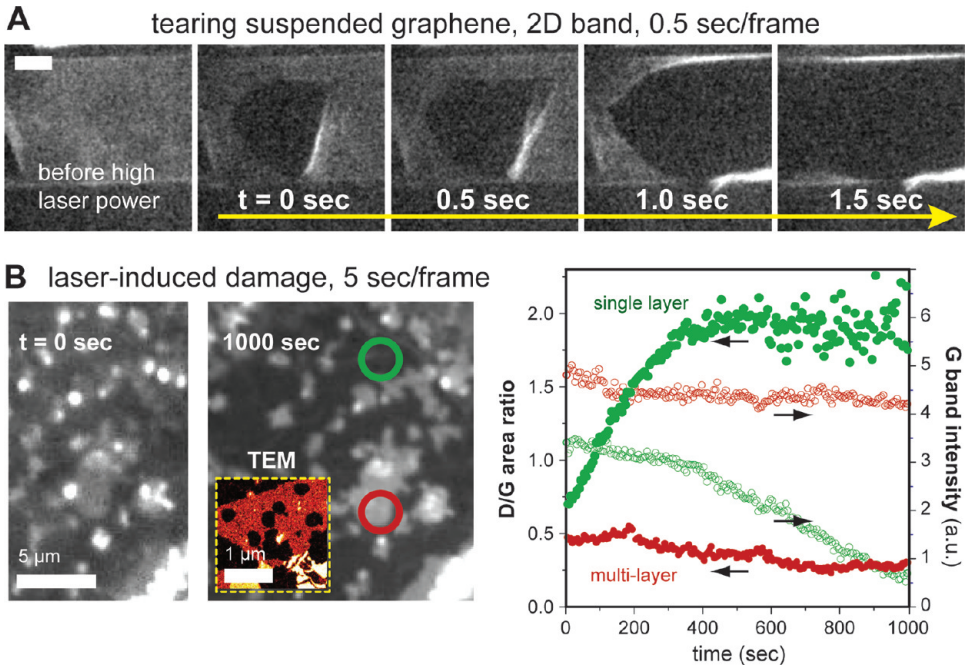

Figure 5. (A) Dynamic imaging of laser-induced tearing of suspended graphene. Images show 2D band of a strip of graphene (bright) suspended between two pieces of silicon (dark). When laser power is increased, a hole forms in the graphene, which eventually causes the graphene strip to mechanically fail. This tearing is observed with 0.5 s resolution. Images are Gaussian blurred (radius 1 pixel =125 nm) to reduce CCD noise. Scale bar is 5 μm. (B) Dynamic spectroscopy along a line of a graphene sample on Si/285 nm oxide. (Left) G band images showing a sample before and after exposure to a 3 W laser. Dark regions appear, showing highly damaged graphene. (Inset) A false color dark-field TEM image (see Methods, Supporting Information) of a similar multilayer sample on thin silicon nitride that has been heavily damaged by the imaging laser, showing circular etch pits indicative of oxidation. (Right) D/G area ratio and G band intensity extracted from spectra taken at locations shown by red and green circles (left). D and G (+ D′) peaks fit to single Lorentzians. Single-layer graphene (green) shows behavior consistent with increasing amorphization with time, but for multilayer graphene (red), the D/G ratio and G intensity remain relatively constant, showing that multilayer graphene is much more resistant to laser-induced damage than single-layer graphene.

our suspended graphene. Our rapid time resolution allows us to see precisely where failures form in our suspended graphene sheets and how they propagate, enabling future studies of this and other interesting dynamic mechanical processes in graphene under a uniform external stress or local AFM indentation.

In addition, imaging spectroscopy can be used to obtain dynamic spectral information for many points on the sample surface simultaneously. When graphene is supported on a substrate, it cannot fail mechanically, but high laser power can cause the graphene to degrade. Laser-induced degradation has been observed previously for a weak laser power (2 mW) over a long time scale (~1 day),[16] but on a silicon/285 nm SiO_2 substrate, a 3 W laser over an 80 μm spot size (~0.5 mW/μm^2) degrades graphene within minutes. G band images of a sample before and after intense laser irradiation (Figure 5B, left) show that the G band intensity decreases significantly over most of the sample after damage. The method in Figure 2D cannot be used to measure the temperature at higher laser powers directly, because hole doping above 200 °C can cause the G peak to redshift,[25] but it is reasonable to assume that the temperature of our samples increases locally by hundreds of degrees Celsius at this laser power, causing the graphene to oxidize. To confirm that oxidation is the primary damage mechanism, a dark-field TEM image[29] of a similar graphene sample on a thin silicon nitride membrane (Figure 5B, inset; see Supporting Information) with extensive laser damage shows circular etch pits in multilayer regions, which is indicative of oxidative damage.[25]

To examine this process in detail, we use imaging spectroscopy (as in Figure 2) to collect Raman spectra every 5 s along a line of the sample shown in Figure 5B. For most of the sample (green), the D/G area ratio increases immediately upon intense laser irradiation up to a value of ~2, after which the G band intensity begins to decrease significantly, consistent with the amorphization of single-layer graphene.[8,32] However, for multilayer areas (red), the G band intensity stays constant with time and the D/G ratio actually decreases slightly. The decreased reactivity of multilayer regions as compared to single-layer regions is consistent with the previous studies of graphene oxidation[25] and chemical reactivity.[33] We stress that with WRI, we obtain dynamic, spectrally resolved information for many points on our sample simultaneously, which cannot be achieved with conventional confocal techniques. An exciting future application of this technique

is spatially and spectrally resolved monitoring of CVD graphene growth *in situ*.

CONCLUSION

In summary, widefield Raman imaging is easily implementable, and can rapidly image and characterize graphene over different length scales while providing detailed spectral resolution. Unlike both white-light imaging and confocal Raman spectroscopy, WRI can be used to map the location of graphene over a large area, and distinguish single- and multilayer regions, on arbitrary substrates within minutes. This technique can easily be extended to locate other Raman-active thin films, such as boron nitride, on arbitrary substrates as well. The ability to rapidly acquire Raman images with high spectral resolution is a powerful characterization tool, allowing us to see spatial variations in film quality that would go unnoticed with point Raman spectroscopy. In addition, the acquisition speed of this technique is fast enough to allow us to observe dynamic processes in graphene with high spatial and spectral resolution. Because optical microscopy can be performed in a variety of environments, this technique enables many *in situ*, time-resolved studies of graphene growth, degradation, and electrical and mechanical processes. We expect that widefield Raman imaging will prove to be an important experimental technique for graphene imaging, enabling large-scale device fabrication and graphene growth characterization.

METHODS

Experimental setup. The Raman setup was built using an IX71 inverted microscope (Olympus) as a platform. A high power, diode-pumped solid state (DPSS) laser (532 nm for all images except Figure 3A, which was obtained with 450 nm laser) was used as an excitation source. The beam was passed through a cleanup bandpass filter and linearly polarized through a polarizing cube, and the beam size was adjusted with a beam expander. A large collimated illumination beam (40−300 μm in diameter) was obtained by focusing the laser at the back focal plane of the objective lens (100× UMPlanFL (N.A.= 0.95) or 20× UPlanApo (N.A.= 0.70), Olympus) using a convex lens (achromat, $f = 200$ mm, Thorlabs). The power delivered to the sample is orders of magnitude greater than that used by confocal Raman techniques (up to hundreds of mW for WRI on graphene *vs* ∼0.1 mW for confocal Raman on graphene), but the power per unit area remains low (∼0.1 mW/μm^2 for both techniques).

The collimated light illuminated the sample and the scattered light was collected *via* the same objective lens, passing through a dichroic beam splitter and long bandpass filter to eliminate the elastically scattered light. The selection of specific Raman bands was performed by either double tunable bandpass filters (see later section) or a single bandpass filter (fwhm=10 nm, Thorlabs) before the light entered an imaging spectrometer (Princeton Instruments). The imaging spectrometer contained a turret with an interchangeable 1200 g/mm, 500 nm blaze grating (spectral mode) and a mirror (imaging mode). Images were recorded using a CCD camera (either 1340 × 400 pixels, 20 μm pixel size, Pixis 400BR, Princeton Instruments, or 1002 × 1004 pixels, 8 μm pixel size, Andor iXon 885 EMCCD) (see Supporting Information for a detailed schematic of the setup, Figure S1).

Tunable Filter Design. We achieved a bandwidth as small as 2.5 nm by using two tunable bandpass filters (TBP01-620/14-25 × 36, Semrock). The individual filters have a ∼20 nm bandwidth, and the center wavelength (CWL) of each bandpass filter can vary from 620 to 550 nm by changing the angle between the filter and the incident light from 0 to 60° (CWL ≈ sin(θ)). By offsetting the two filters about 10° apart, the two bandpass filters act as one narrow tunable filter, with a roughly constant 2.5 nm fwhm between 560 and 590 nm, the range where CWL *vs* θ is approximately linear. For wavelengths above 600 nm, the bandwidth increases, reaching ∼20 at 620 nm (2D band @ 532 nm excitation) (see Supporting Information for filter image and transmission data, Figure S2).

Dark Field TEM Imaging. Dark field TEM imaging was performed using the method outlined by Huang *et al.*[29] (see Supporting Information for more information about data acquisition and interpretation).

Carbon Nanotube Synthesis. Microfabrication was performed using conventional photolithography on commercially available ST-cut quartz wafers (Hoffman Materials, LLC), according to procedures previously reported in the literature.[34] Catalyst line features were defined and ∼2 Å of Fe was deposited by e-beam evaporation. Following lift-off, the substrates were placed in a quartz reaction tube and annealed in air at 900 °C for 9 h. Without cooling, aligned SWNTs were grown using a procedure adapted from Kocabas *et al.* at 900 °C using methane as the carbon feedstock.[34]

Graphene Synthesis. Large-area graphene samples were grown on metal substrates using previously reported CVD techniques.[2,35] Growth of graphene on Cu foil (99.8% Alfa Aesar no. 13382) was conducted inside a hot wall tube furnace, which was heated while flowing H_2 (ultra high purity grade; Air Gas, Inc.) and CH_4 (ultra high purity grade, Air Gas, Inc.). Growth parameters (temperature, flow rates, time) were varied as follows. Figures 1 and 3C: 980 °C, 120 sccm flow of H_2, 1 sccm of CH_4, 70 min. Growth was conducted inside a Cu enclosure that was inserted into the furnace.[35] Figures 2, 3A,E, and 4A: 980 °C, 60 sccm of H_2, 1 sccm of CH_4, 90 min. Growth was conducted inside a Cu enclosure that was inserted into the furnace (Kevek Innovations 1 in. CVD system). Figures 3B, 4C, and 5A: 980 °C, 300 sccm of H_2, 875 sccm of CH_4, 20 min. Growth was conducted inside a Cu enclosure that was inserted into the furnace. Figure 3D: 980 °C, 60 sccm of H_2, 1 sccm of CH_4, 100 min. Growth was conducted inside a Cu enclosure that was inserted into the furnace (Kevek Innovations 1 in. CVD system). Figure 4B: 1000 °C, 100 sccm of H_2, 3 sccm of CH_4, 10 min. Cu was cleaned with an oxygen plasma before growth. Figure 4D: 1000 °C, 300 sccm of H_2, 875 sccm of CH_4, 13 h. Figure 5B: 1000 °C, 300 sccm of H_2, 875 sccm of CH_4, 13 min.

Graphene Transfer. Synthesized graphene on copper was transferred to various other substrates with the following process. First, protective poly(methylmethacrylate) (PMMA, 2% 495K in anisole) was spin-coated onto the Cu/graphene substrate. The Cu/graphene substrate was floated on a dilute aqueous iron(III) chloride solution ($FeCl_3$, Aldrich) in order to etch the Cu from the back. The remaining PMMA/graphene membrane was gently washed with copious amounts of water and was transferred onto the target substrate. The transferred substrate was gently dried to remove any water. Finally, the PMMA was removed in acetone or 1165 stripper (Shipley), and the substrate was washed with IPA and dried with N_2 gas (for suspended samples, a critical drying process was used).

Acknowledgment. The authors thank L. Herman, M. P. Levendorf, and J. Kevek for help with sample fabrication. This work was mainly supported by the NSF-funded Center for Chemical Innovation and the Air Force Office of Scientific Research. Additional funding was received from the NSF through the

Center for Nanoscale Systems, Cornell Center for Materials Research, Alfred P. Sloan Foundation, and NSF CAREER grant. Sample fabrication was performed at the Cornell Nanoscale Science and Technology Facility, a National Nanotechnology Infrastructure Network node. This work made use of the TEM facility of the Cornell Center for Materials Research (CCMR) with support from the National Science Foundation Materials Research Science and Engineering Centers (MRSEC) program (DMR 1120296). R. W. Havener is supported by a Graduate Research Fellowship from the National Science Foundation. S.-Y. Ju received financial support from the Yonsei University Research Fund of 2011.

Supporting Information Available: PDF file containing a schematic of the experimental setup, transmission data for tunable bandpass filter, image processing procedures, and dark-field TEM imaging details; a video of laser-induced tearing of suspended graphene. This material is available free of charge *via* the Internet at http://pubs.acs.org.

REFERENCES AND NOTES

1. Geim, A. K. Graphene: Status and Prospects. *Science* **2009**, *324*, 1530–1534.
2. Li, X.; Cai, W.; An, J.; Kim, S.; Nah, J.; Yang, D.; Piner, R.; Velamakanni, A.; Jung, I.; Tutuc, E.; *et al*. Large-Area Synthesis of High-Quality and Uniform Graphene Films on Copper Foils. *Science* **2009**, *324*, 1312–1314.
3. Reina, A.; Jia, X.; Ho, J.; Nezich, D.; Son, H.; Bulovic, V.; Dresselhaus, M.; Kong, J. Large Area, Few-Layer Graphene Films on Arbitrary Substrates by Chemical Vapor Deposition. *Nano Lett.* **2009**, *9*, 30–35.
4. Blake, P.; Hill, E.; Neto, A.; Novoselov, K.; Jiang, D.; Yang, R.; Booth, T.; Geim, A. Making Graphene Visible. *Appl. Phys. Lett.* **2007**, *91*, 063124.
5. Stohr, R.; Kolesov, R.; Pflaum, J.; Wrachtrup, J. Fluorescence of Laser-Created Electron-Hole Plasma in Graphene. *Phys. Rev. B* **2010**, *82*, 121408.
6. Kim, J.; Cote, L.; Kim, F.; Huang, J. Visualizing Graphene Based Sheets by Fluorescence Quenching Microscopy. *J. Am. Chem. Soc.* **2010**, *132*, 260–267.
7. Maciel, I. O.; Anderson, N.; Pimenta, M. A.; Hartschuh, A.; Qian, H.; Terrones, M.; Terrones, H.; Campos-Delgado, J.; Rao, A. M.; Novotny, L.; *et al*. Electron and Phonon Renormalization Near Charged Defects in Carbon Nanotubes. *Nat. Mater.* **2008**, *7*, 878–883.
8. Ferrari, A.; Robertson, J. Interpretation of Raman Spectra of Disordered and Amorphous Carbon. *Phys. Rev. B* **2000**, *61*, 14095–14107.
9. Graf, D.; Molitor, F.; Ensslin, K.; Stampfer, C.; Jungen, A.; Hierold, C.; Wirtz, L. Spatially Resolved Raman Spectroscopy of Single- and Few-Layer Graphene. *Nano Lett.* **2007**, *7*, 238–242.
10. Das, A.; Pisana, S.; Chakraborty, B.; Piscanec, S.; Saha, S.; Waghmare, U.; Novoselov, K.; Krishnamurthy, H.; Geim, A.; Ferrari, A.; *et al*. Monitoring Dopants by Raman Scattering in an Electrochemically Top-Gated Graphene Transistor. *Nat. Nanotechnol.* **2008**, *3*, 210–215.
11. Ferrari, A. C. Raman Spectroscopy of Graphene and Graphite: Disorder, Electron-Phonon Coupling, Doping and Nonadiabatic Effects. *Solid State Commun.* **2007**, *143*, 47–57.
12. Malard, L.; Pimenta, M.; Dresselhaus, G.; Dresselhaus, M. Raman Spectroscopy in Graphene. *Phys. Rep.* **2009**, *473*, 51–87.
13. Mohiuddin, T. M. G.; Lombardo, A.; Nair, R. R.; Bonetti, A.; Savini, G.; Jalil, R.; Bonini, N.; Basko, D. M.; Galiotis, C.; Marzari, N.; *et al*. Uniaxial Strain in Graphene by Raman Spectroscopy: G Peak Splitting, Gruneisen Parameters, and Sample Orientation. *Phys. Rev. B* **2009**, *79*, 205433.
14. Dresselhaus, M.; Dresselhaus, G.; Saito, R.; Jorio, A. Raman Spectroscopy of Carbon Nanotubes. *Phys. Rep.* **2005**, *409*, 47–99.
15. Ferrari, A.; Meyer, J.; Scardaci, V.; Casiraghi, C.; Lazzeri, M.; Mauri, F.; Piscanec, S.; Jiang, D.; Novoselov, K.; Roth, S.; *et al*. Raman Spectrum of Graphene and Graphene Layers. *Phys. Rev. Lett.* **2006**, *97*), 187401.
16. Krauss, B.; Lohmann, T.; Chae, D.; Haluska, M.; von Klitzing, K.; Smet, J. Laser-Induced Disassembly of a Graphene Single Crystal Into a Nanocrystalline Network. *Phys. Rev. B* **2009**, *79*, 165428.
17. Batchelder, D.; Cheng, C.; Muller, W.; Smith, B. A Compact Raman Microprobe Microscope—Analysis of Polydiacetylene Langmuir and Langmuir−Blodgett Films. *Makromol. Chem., Macromol. Symp.* **1991**, *46*, 171–179.
18. Treado, P.; Levin, I.; Lewis, E. High-Fidelity Raman Imaging Spectrometry—A Rapid Method Using an Acoustooptic Tunable Filter. *Appl. Spectrosc.* **1992**, *46*, 1211–1216.
19. Puppels, G.; Grond, M.; Greve, J. Direct Imaging Raman Microscope Based on Tunable Wavelength Excitation and Narrow-Band Emission Detection. *Appl. Spectrosc.* **1993**, *47*, 1256–1267.
20. Schlucker, S.; Schaeberle, M.; Huffman, S.; Levin, I. Raman Microspectroscopy: A Comparison of Point, Line, and Wide-Field Imaging Methodologies. *Anal. Chem.* **2003**, *75*, 4312–4318.
21. Kaminska, K.; Lefebvre, J.; Austing, D.; Finnie, P. Real-Time Global Raman Imaging and Optical Manipulation of Suspended Carbon Nanotubes. *Phys. Rev. B* **2006**, *73*, 235410.
22. Kaminska, K.; Lefebvre, J.; Austing, D. G.; Finnie, P. Real-Time *in Situ* Raman Imaging of Carbon Nanotube Growth. *Nanotechnology* **2007**, *18*, 165707.
23. Bowden, M.; Gardiner, D.; Rice, G.; Gerrard, D. Line-Scanned Micro Raman Spectroscopy Using a Cooled CCD Imaging Detector. *J. Raman Spectrosc.* **1990**, *21*, 37–41.
24. Wang, Y.; Ni, Z.; Shen, Z.; Wang, H.; Wu, Y. Interference Enhancement of Raman Signal of Graphene. *Appl. Phys. Lett.* **2008**, *92*, 043121.
25. Liu, L.; Ryu, S.; Tomasik, M.; Stolyarova, E.; Jung, N.; Hybertsen, M.; Steigerwald, M.; Brus, L.; Flynn, G. Graphene Oxidation: Thickness-Dependent Etching and Strong Chemical Doping. *Nano Lett.* **2008**, *8*, 1965–1970.
26. Cai, W.; Moore, A.; Zhu, Y.; Li, X.; Chen, S.; Shi, L.; Ruoff, R. Thermal Transport in Suspended and Supported Monolayer Graphene Grown by Chemical Vapor Deposition. *Nano Lett.* **2010**, *10*, 1645–1651.
27. Zhang, Y.; Son, H.; Zhang, J.; Dresselhaus, M.; Kong, J.; Liu, Z. Raman Spectra Variation of Partially Suspended Individual Single-Walled Carbon Nanotubes. *J. Phys. Chem. C* **2007**, *111*, 1983–1987.
28. Wang, Y.; Ni, Z.; Yu, T.; Shen, Z.; Wang, H.; Wu, Y.; Chen, W.; Wee, A. Raman Studies of Monolayer Graphene: The Substrate Effect. *J. Phys. Chem. C* **2008**, *112*, 10637–10640.
29. Huang, P.; Ruiz-Vargas, C.; van der Zande, A.; Whitney, W.; Levendorf, M.; Kevek, J.; Garg, S.; Alden, J.; Hustedt, C.; Zhu, Y.; *et al*. Grains and Grain Boundaries in Single-Layer Graphene Atomic Patchwork Quilts. *Nature* **2011**, *469* 389–392.
30. Chen, S.; Brown, L.; Levendorf, M.; Cai, W.; Ju, S.; Edgeworth, J.; Li, X.; Magnuson, C.; Velamakanni, A.; Piner, R.; *et al*. Oxidation Resistance of Graphene-Coated Cu and Cu/Ni Alloy. *ACS Nano* **2011**, *5*, 1321–1327.
31. Boyd, G.; Yu, Z.; Shen, Y. Photoinduced Luminescence From the Noble Metals and Its Enhancement on Roughened Surfaces. *Phys. Rev. B* **1986**, *33*, 7923–7936.
32. Ferreira, E.; Moutinho, M.; Stavale, F.; Lucchese, M.; Capaz, R.; Achete, C.; Jorio, A. Evolution of the Raman Spectra from Single-, Few-, and Many-Layer Graphene with Increasing Disorder. *Phys. Rev. B* **2010**, *82*, 125429.
33. Sharma, R.; Baik, J.; Perera, C.; Strano, M. Anomalously Large Reactivity of Single Graphene Layers and Edges toward Electron Transfer Chemistries. *Nano Lett.* **2010**, *10*, 398–405.
34. Kocabas, C.; Kang, S.; Ozel, T.; Shim, M.; Rogers, J. Improved Synthesis of Aligned Arrays of Single-Walled Carbon Nanotubes and Their Implementation in Thin Film Type Transistors. *J. Phys. Chem. C* **2007**, *111*, 17879–17886.
35. Li, X.; Magnuson, C.; Venugopal, A.; Tromp, R.; Hannon, J.; Vogel, E.; Colombo, L.; Ruoff, R. Large-Area Graphene Single Crystals Grown by Low-Pressure Chemical Vapor Deposition of Methane on Copper. *J. Am. Chem. Soc.* **2011**, *133*, 2816–2819.